International Journal of Thermofluids 7–8 (2020) 100018

Contents lists available at ScienceDirect

International Journal of Thermofluids

journal homepage: www.elsevier.com/locate/ijtf

Experimental and numerical analysis of a liquid aluminium injector for an Al-H_2O based hydrogen production system

Massimo Milani[a], Luca Montorsi[a,*], Gabriele Storchi[a], Matteo Venturelli[a], Diego Angeli[a], Adriano Leonforte[a], Davide Castagnetti[a], Andrea Sorrentino[a]

[a] Department of Sciences and Methods for Engineering, University of Modena and Reggio Emilia, Italy

ARTICLE INFO

Article History:
Received 11 December 2019
Revised 26 January 2020
Accepted 28 January 2020
Available online 31 January 2020

Keywords:
Hydrogen generation
Aluminium-water reaction
Experiments
Simulation
Structural and thermal analysis

ABSTRACT

This paper investigates pressurised injection system for liquid aluminium for a cogeneration system based on the Al−H_2O reaction. The reaction produces hydrogen and heat which is used for super-heating vapour for a steam cycle. The aluminium combustion with water generates also alumina as a byproduct; the aluminium oxide can be recycled and transformed back to aluminium. Thus, aluminium can be exploited as energy carrier in order to transport energy from the alumina recycling plant to the place where the cogeneration system is located. The water is also used in a closed loop; indeed, the amount of water produced employing the hydrogen obtained by the proposed system corresponds to the oxidizing water for the Al/H_2O reaction. The development of a specific test rig designed for investigating the liquid aluminium injection is presented in this research study. The injector nozzle is investigated by means of numerical thermal and structural analysis. The calculations are compared and validated against the experimental measurements carried out on ad-hoc developed test rig. A good agreement between the numerical results and the experimental values is found and the new design of the nozzle is devised.

1. Introduction

In the European Union, it is estimated that around three quarters of the energy consumption comes from non-renewable resources [1]. Within this context, the constant increase in the air pollution and carbon emission has led the competent Institutions and the scientific community in finding sustainable solutions and policies to reduce the environmental impact of the human activities.

In this regard, improvement in energy efficiency for the technologies already available and the development of green energy systems capable to replace the fossil fuels can be identified as possible solutions for a cleaner energy economy distinguished by lower emissions.

Malinauskaite et al. [1] presented a review of the European strategies and policies that can be considered the main drivers to reduce the emissions by means of the improvement of energy efficiency and by encouraging the use of renewable sources.

Possible paths for a sustainable energy development were highlighted in [2]. Lior [2] presented a discussion related to the prospects of the main energy sources, i.e., fossil, nuclear and renewable energy, and related to the power generation, including hydrogen, fuel cells and micro-power system. Higher energy conversion efficiency, elimination of obvious waste, less-energy demanding lifestyles and recycling are general rules for a wiser use of energy sources. The study concluded that the research and development of technologies based on renewable sources must continue incessantly, and it must be applied to every sector: transportation, buildings, industry. The implementation of these systems and the development of new materials that would reduce the energy losses are some of the ingredients of the sustainable energy economy recipe.

Jouhara et al. [3] focused on the industrial sector and presented a review related to the waste heat technologies that can be applied in the industrial context in order to reduce the waste heat that is not put into practical use. The study investigated the performance and the working principles and functionalities of the main waste heat technologies such as heat exchangers, recuperators, regenerators, recuperative burners, heat pumps, heat pipe systems and heat recovery steam generators. An application of these technologies in different industrial context can be also found in [4].

As already mentioned, with the rising consciousness about the limit of the fossil fuels the scientific community is challenged in developing more sustainable energy carriers. Hydrogen can be regarded as one of the most attracting energy carriers that will determine a decrease in the environmental impact; indeed, hydrogen and fuel cells are considered as one of the energy solutions for the 21st century [5].

* Corresponding author.
E-mail address: luca.montorsi@unimore.it (L. Montorsi).

https://doi.org/10.1016/j.ijft.2020.100018

In literature, there are many research works that have explored the use of hydrogen in different applications [6]. Sharma and Ghoshal [7] investigated the application of hydrogen to power vehicles for the generation of a zero-emission transportation. In [8] the use of liquid hydrogen as a potential substitute of kerosene is analysed for aviation application while Sorgulu and Dincer [9] developed an integrated based hydrogen energy system for residential application.

Nowadays, hydrogen can be produced from varieties of processes including fossils and renewable sources [7]. An in-depth review of the main technologies for the hydrogen production is reported in [10]. The main methodologies mentioned in the study included: steam methane reforming, gasification of coal or other hydrocarbons, electrolysis of water and hydrogen production from biomass or nuclear energy. Most of the mentioned techniques can be considered responsible for the greenhouses gases emission; indeed, natural gas steam reforming produces CO_2 emission at a rate close to 7.5 kg CO_2/kg H_2 [11]. The low density of hydrogen is a critical issue for the gas storage and, then, it is not easy to transport [12]; therefore, the storage and delivery cost are unacceptable for many energy applications.

A promising methodology to avoid these issues comes from the metal reaction with water for generating hydrogen without greenhouse gases emissions; the metal is used as energy carrier [13]. Metal-water reaction exhibits many advantages such as the possibility to produce hydrogen on demand and it is safe and inexpensive since it overcomes the issues related to the hydrogen cooling and pressurization [14]. In particular, the aluminium combustion with water has been widely investigated in literature and most of the studies are applied to the marine application [15] and rockets propellants [16]. The liquid aluminium reaction with water for hydrogen production can take place at low temperatures applying expensive alloying agents or it can be activated using high-temperatures reactors [17].

When investigating the reaction at high temperature, the researchers' attention is mainly focused on the aluminium powders that are generated in a different chamber detached from the one where the reaction occurs [18,19]; indeed, many studies investigated the aluminium particles combustion with water [20,21].

The use of molten aluminium to activate the reaction displays many advantages because it helps to overcome the issues of producing the aluminium powder, and it enables to design a cogeneration system based on the combustion of scrap aluminium with water [22].

The aim of this study is the design of a test rig to investigate the liquid aluminium reaction with water that have been extensively described in [23,24]. The experimental apparatus is equal to 1:10 with the respect to the system defined as layout D analysed in [25].

Special attention is devoted here to thermomechanical loads, which are critical for many structures and mechanical components [26]. The design of the test rig, and in particular of the injector section, envisages the coupling of three components, made of different materials, whose thermal and mechanical behaviour is to be investigated to ensure structural integrity under the extreme thermal loads to which the system is subjected, especially during heating and cooling transients. Although analytical solutions of transient thermal conduction problems might be obtained for simple geometries but with arbitrarily complex time-varying boundary conditions [27], the presence of multiple materials and non-trivial geometries entails the resort to numerical solutions of the heat equation. To this aim, a thermal simulation of the heating and cooling phases of the system has been carried out, restricted to injector section.

The results from the computational thermal analysis have been implemented in a thermomechanical model that applies the previously calculated temperature map to the structure and calculates the mechanical response of the system, with particular care to the stresses and strains. The results show that in steady state condition, the stresses on the system are quite low, thanks to a favourable difference between the thermal expansion coefficients of the three components: the outer threaded nut has the higher thermal expansion coefficient, followed by the nozzle and by the graphite melting pot.

2. Materials and methods

This paper presents the design of a test rig for the investigation of the aluminium spray for a liquid aluminium injector for an Al-H_2O combustion chamber. This novel concept of burner is aimed at equipping a cogeneration system based on molten aluminium combustion with water to produce hydrogen and heat. The system is potentially able to generate simultaneously hydrogen, thermal power and electric energy in a fully environment sustainable manner. The system is based on a new type of combustor capable of injecting liquid aluminium in a slightly superheating steam stream, the resulting reaction provides the heat for the cogeneration system and the only by product is the aluminium oxide. In fact, the oxidation reaction of the metallic fuel with water is highly exothermic and when it stabilizes it becomes the energy source for a cogeneration system providing multiple secondary energy sources. When Aluminium is assumed as the baseline metallic fuel, its oxidation reaction with water begins at ambient condition and releases an amount of energy equal to approximately 18 MJ per kilogram of solid fuel along with gaseous hydrogen (as the main combustion product) and superheated steam. Both the hydrogen and the superheated steam can be employed in turbine producing mechanical work (which can be eventually collected at the crankshaft) and electric energy (by connecting an alternator to the turbine crankshaft) and heat (which can be used in industrial or civil combined heat and power energy systems). The metallic fuel oxidation process does not produce carbon monoxide or any other pollutant emission. Furthermore, the waste products of the combustion can be recycled, in fact they are found in the crystalline state (likely with very small and highly pure crystals) and can be easily removed continuously or during maintenance and afterword it can be utilised in hi-tech applications or reconverted into pure metallic fuel.

From the viewpoint of the environmental impact, the main advantages of the energy conversion system based on this novel technology lie essentially in the opportunity of realizing a closed life cycle which in principle eliminates the necessity of providing new fuel, i.e., aluminium, once the waste products are recycled. Within this scenario the aluminium becomes an energy carrier that can transport renewable energy where it is mostly available to the place where it can be exploited. Similarly, the oxidizer, i.e., water, in a closed life cycle can be recovered and only the leaked amount has to be restored. More details about the system can be found in [24,25].

The aim of the paper is the improvement of a test rig for the experimental analysis of the cogeneration system to assess the performance in terms of hydrogen production, energy efficiency and the sustainability of the process.

2.1. Experimental test rig

The system is fed with aluminium wires. The experimental apparatus includes a melting furnace, a tank, a water pump and a separate system with nitrogen pressurised in order to facilitate the aluminium injecting phase.

Fig. 1 depicts the experimental apparatus assembled for the investigation.

The main unit is the graphite crucible where the aluminium is melted thanks to the inductive melting furnace. The maximum temperature that can be reached in the unit is 1300 °C. The crucible where the aluminium melting takes place is pressurised by nitrogen which is an inert gas able to prevents uncontrolled oxidation that an interaction with the external atmosphere could develop.

The aluminium reaches the desired temperature for the injection heated up by means of two induction elements. A cooling system composed by demineralised cold water avoids the overheating of the

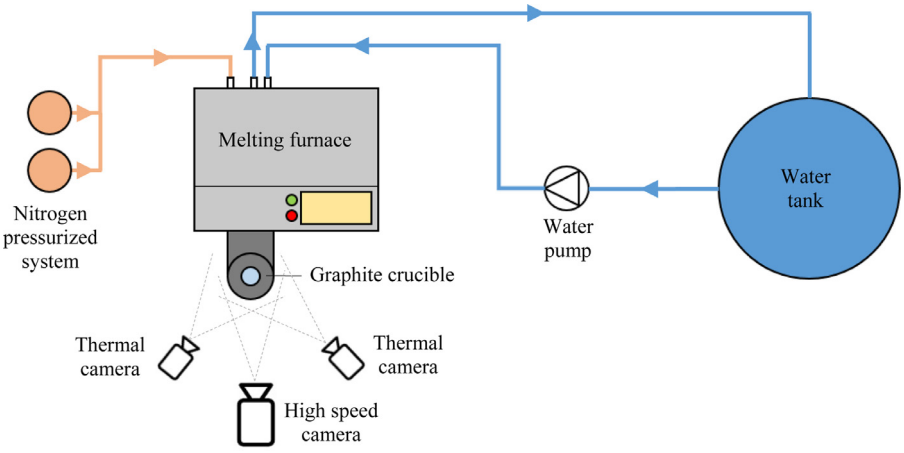

Fig. 1. Schematic of the experimental apparatus.

furnace; a water pump supplies the cooling fluid in the circuit from a tank filled at the beginning of the experimental test.

The injection phase is regulated by a graphite pneumatic needle valve. When the warm up phase finishes, the thermodynamic equilibrium between the injector and the molten aluminium is reached. Thus, it can be assumed that the temperature of the injector is equal to the temperature of the liquid aluminium injection. The liquid aluminium injection rate is monitored by an integrated PLC system installed on the furnace that controls the nitrogen pressure and the needle lift. The system can also regulate the nitrogen pressure up to 6 bar in order to keep under control the liquid aluminium injection pressure.

The PLC system is also capable to regulate the electric current of each inductive element in order to keep the injection temperature of the molten aluminium constant to a set value along the entire injection system (injector and graphite crucible).

The sensors installed in the system are employed to monitor the main variable of the process.

Three thermocouples (A) are installed into the furnace in three different positions in order to monitor the temperature distribution inside the furnace and define the thermal behaviour of the melting furnace. These sensors enable to investigate the three different temperatures during the whole execution of the experimental test.

Two thermal cameras (B) and the high velocity camera (C) are positioned in front of the experimental apparatus. The thermal cameras are used to register the temperature profile of the inlet whereas the velocity of the aluminium spray during the injecting phase is captured by the high velocity camera. The thermal cameras have two different operative ranges in order to monitor the whole heating up phase.

Fig. 2(a) illustrates the positioning of the three thermocouples inside the furnace cavity while 2(b) shows the installation of the three cameras in front of the system.

Table 1 lists the operating range and the accuracy of the measuring instruments employed to characterise the system.

A National Instrument DAQ module integrated by a customised LabView interface has been used to acquire the experimental data. The LabView control panel enables the user to control remotely all the working parameters of the system.

2.2. Simulation of the thermal transient

In order to investigate the evolution of the temperature distribution in the injector section, a computational model has been set up to solve the transient, pure conduction problem in a specific subdomain of the designed test rig, depicted in Fig. 3(a). The model includes: (i) the final part of the graphite crucible; (ii) the injection channel (supposed to be filled with air during both heating and cooling phases); (iii) the silicon carbide nozzle; (iv) the titanium threaded nut and (v) the outer steel frame. With reference to the considered subdomain, axial symmetry can be exploited to reduce the model to the cross-section represented in Fig. 3(b). The model has been implemented through the commercial CFD package Ansys® Fluent 18.1 [28]. The final computational mesh of the cross section is composed of 83,000 quadrilateral cells.

Fig. 3(c) reports a summary of the thermal boundary conditions and source terms imposed for the simulations. The outer surfaces of the graphite crucible, the surfaces of the nozzle and threaded nut

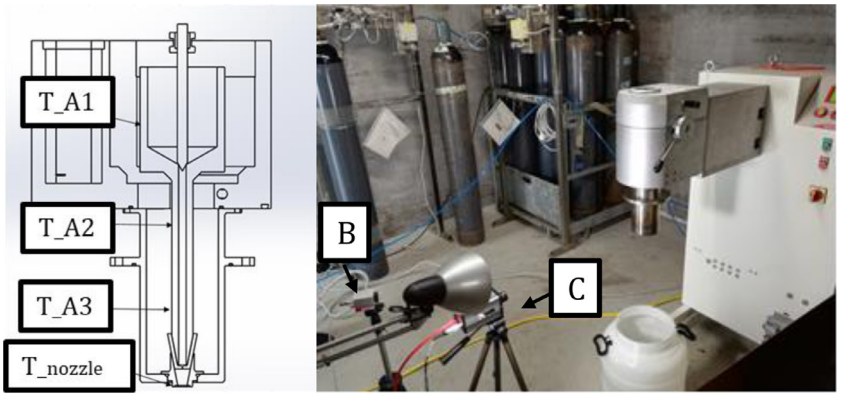

(a) Thermocouple positioning, **(b)** Installation of the three cameras

Fig. 2. (a) Thermocouple positioning, (b) installation of the three cameras.

Table 1
Specifications of the sensors and devices installed.

Sensor type	Operating range	Accuracy	Reference letter in Fig. 1
Thermocouples (Type K)	−270 ÷ 1370 °C		A
Thermal camera	0 ÷ 250 °C	±2%	B
Thermal camera	200 ÷ 1500 °C	±2%	B
High velocity camera	Max 1200 fps		C

Table 2
Thermal properties of the system.

Part	Material	Density [kg m^{-3}]	Specific heat capacity [J kg^{-1} K^{-1}]	Thermal conductivity [W m^{-1} K^{-1}]
Nozzle	carbide ceramic	2000	795.5	1.2
Crucible	graphite	2200	1633	4.9
Threaded nut	titanium	4850	544.3	7.44
Outer frame	steel	8030	502.5	30
Internal channel	air	1.225	1006	0.023

(blue line in Fig. 3c) are considered as adiabatic boundaries during the heating process due to the fact that they are not exposed to the ambient air, indeed, the heat released to the surrounding components can be considered negligible with respect to the heat generated by the inductor. A mixed condition with a constant heat transfer coefficient is used instead during the cooling phase to account for the heat flux in the radial direction. A convective condition is used as well on the outer surfaces of the nozzle, the threaded nut and the steel frame (green line in Fig.3c). For both boundaries the heat transfer coefficient is set as h = 2 (W m^{-2} K), representative of natural convection from a horizontal surface heated from above [29] and the environment temperature equal to T_{env} = 10 °C. A volumetric thermal source q_{gen} is introduced in the graphite domain, to simulate the heat generated by induction. The source term is differentiated in the two regions represented in Fig. 3(c), as it is assumed that less heat is generated in the region enclosed by the nozzle cone. The two sources are set to $q_{gen,1}$ = 12 (MW m^{-3}) and $q_{gen,2}$ = 2.4 (MW m^{-3}), respectively. The two values are a result of a preliminary estimate based on experimental observations. In particular, since it is impossible to determine, either by theoretical or experimental means, the amount of thermal power generated by induction in the aluminium, these values have been tuned based on the temperature measurements reported in Fig. 5, so as to reproduce the heating transient as reasonably as possible. Air in the central channel is considered as still, and thus no convective flows are simulated.

Table 2 reports the thermal properties employed throughout the simulations. Second order schemes are used for time and space integration, and a time step size of 10 s has been deemed as appropriate for the present analysis.

2.3. Thermomechanical analysis

The thermomechanical model imports the nodal temperature distribution calculated in the thermal analysis in order to investigate the stress state in the system. Specifically, the model aims to predict the thermo-mechanical stresses in the nozzle, which is the most critical part of the system, both during heating and cooling transients and in the steady state high temperature working condition.

Fig. 4 shows the axisymmetric finite element (FE) model of the system implemented through the commercial FE software Abaqus 6.16 [30]: the model includes the nose of the melting pot, the nozzle, and the threaded nut that fix the nozzle to the frame. It has been decided to neglect the frame in the FE model, since its effect can be

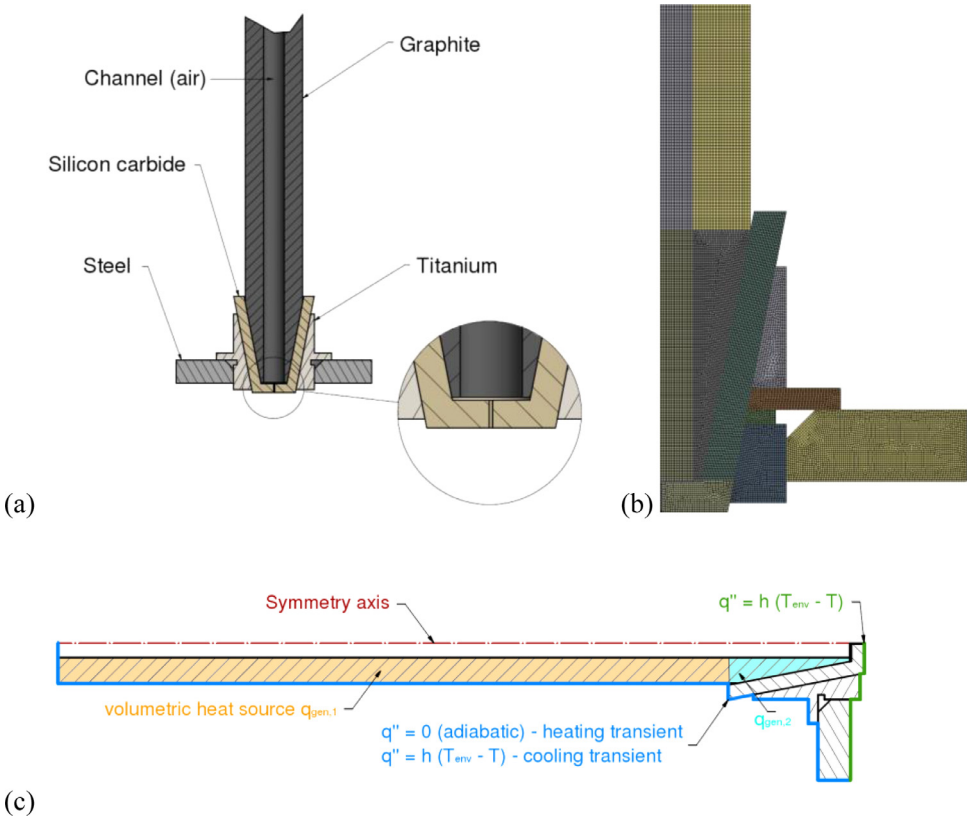

Fig. 3. Thermal simulation of the injector section: (a) detail of the geometrical model of the part, with indication of different materials; (b) axisymmetric computational model and mesh; (c) indication of thermal boundary conditions and sources. (For interpretation of the references to colour in this figure, the reader is referred to the web version of this article.)

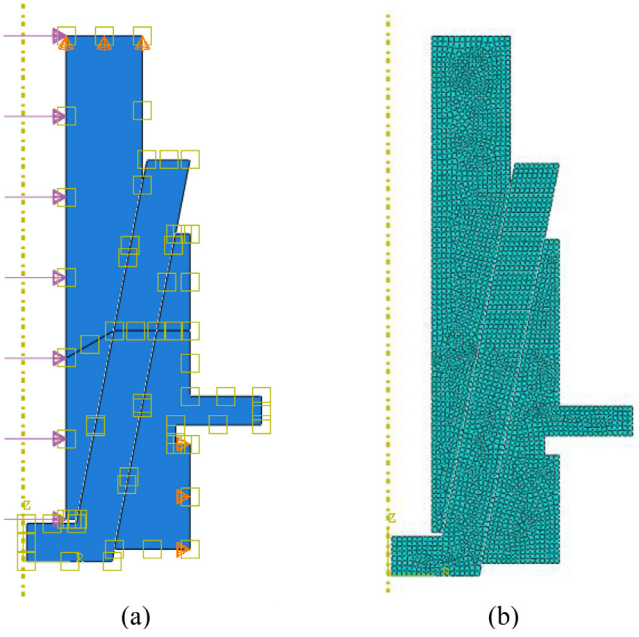

Fig. 4. Axisymmetric FE model of the system with the applied load, mechanical boundary conditions and thermal boundary conditions (a) and mesh of the model (b).

simply and accurately reproduced by applying appropriate constraints on the threaded nut (see below).

The mesh consists of 2D, linear, axisymmetric, triangular, elements (CAX6MT [26]), specific for thermal-displacement analysis (Fig. 4b): the average side length is equal to 1 mm, for a total of 147,405 degrees of freedom. Table 3 reports the material properties of each of the three components.

In order to avoid excessive constraints, the model applies a simple support in the horizontal direction (Fig. 4a) along the lower face of the threaded nut, to reproduce the threaded connection, and a simple support in the vertical direction (Fig. 4a), to reproduce the remaining part of the melting pot. An inner pressure equal to 5 bar was applied

Table 3
Material properties of the system.

Part	Material	Young Modulus (Pa)	Poisson ratio	Thermal Expansion Coefficient (K^{-1})
Nozzle	carbide ceramic	$440000e^6$	0.17	$4.4e^{-6}$
Melting pot	graphite	$27600e^6$	0.23	$5.2e^{-6}$
Threaded nut	titanium	$105000e^6$	0.36	$9.3e^{-6}$

on the inner surface of the nose (Fig. 4a), that correspond to the pressure of the melted aluminium flowing inside the nose. On the inner nodes of the model, it has been applied the temperature distribution retrieved from the thermal analysis step. At the interface between the melting pot and the nozzle, and between the nozzle and the threaded nut, it has been implemented a master-slave contact interaction that describes both the normal behaviour, in terms of contact pressure, and the thermal conductance, due to temperature gradient between the mating parts. The thermomechanical analysis provided the thermo-mechanical stresses acting on the system.

3. Results and discussion

3.1. Experimental measurements on the injection system test rig

In the following, the results of the experimental campaign on the injection system test rig are presented and discussed in terms of temperature distribution in the nozzle, spray formation and analysis of the aluminium particles obtained.

3.2. Temperature analysis

The experimental test presented and described in the previous paragraphs is used for investigating the operating parameters in terms of temperature distribution for the injection process.

In Fig. 5 the temperatures of the three thermocouples installed into the melting furnace and the nozzle's one detected by the

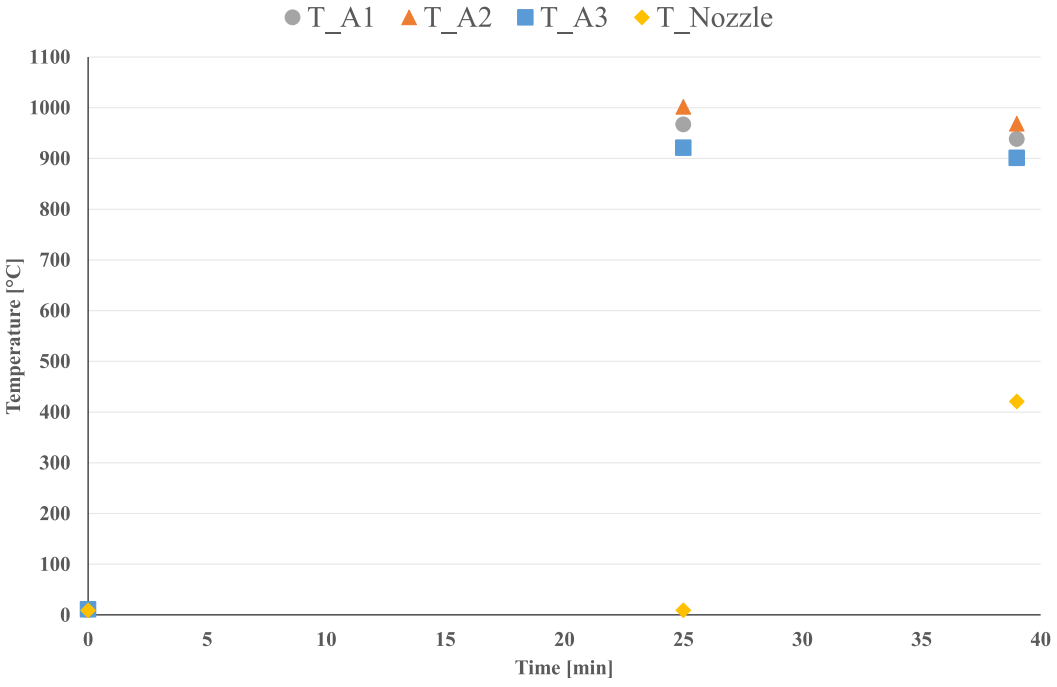

Fig. 5. Temperature profiles monitored by the sensors.

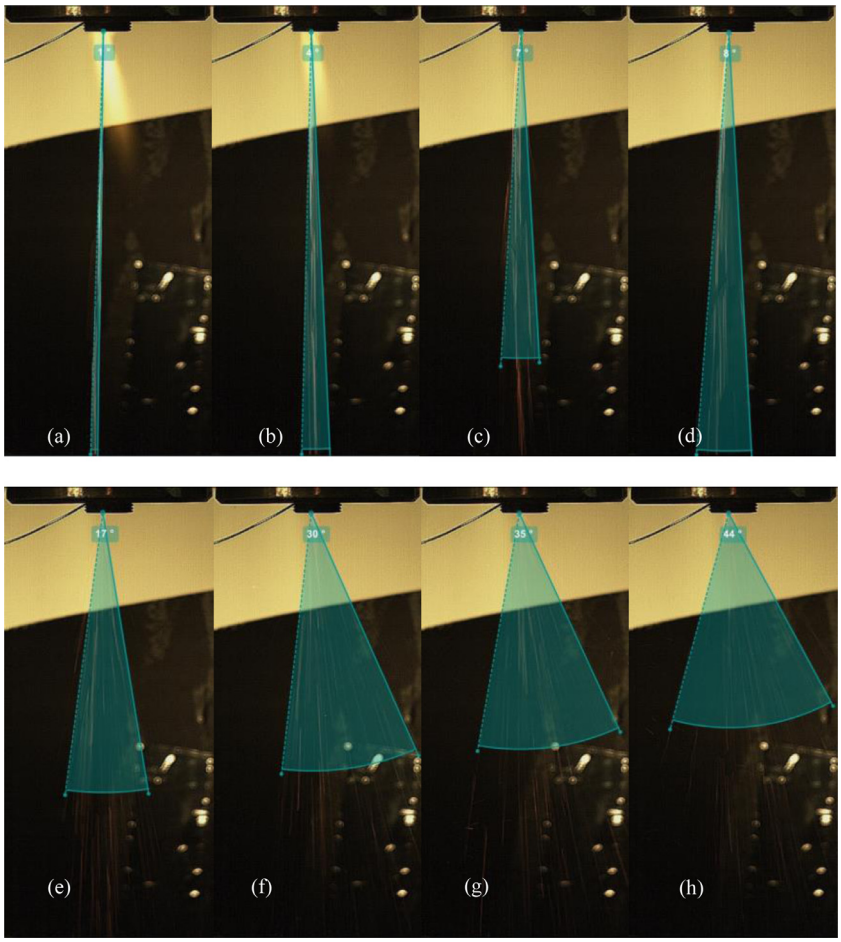

Fig. 6. Aluminium spray angle. (a) Frame #230, (b) Frame #920, (c) Frame #1610, (d) Frame #2300, (e) Frame #2990, (f) Frame #3680, (g) Frame #4370, (h) Frame #5060.

thermal camera installed in front of the experimental apparatus are depicted. During the heating of the melting furnace very similar values are registered by the three thermocouples, i.e., TA1, TA2, TA3, because they are near the two induction elements. The last value depicted in the figure below (T_Nozzle) is the value registered by the thermal camera and represents the temperature of the nozzle from which the aluminium flows out. T_Nozzle has this particular profile because the first two points are taken at the beginning of the experimental test (induction elements turned off) and at the end of the heating up phase while the third one is registered just before the aluminium injection.

3.3. Aluminium spray angle

The second parameter investigated in the paper is the exit angle of the aluminium spray during the injecting phase. Using the high velocity camera shown in Fig. 2b, high resolution frames taken at different instants of time can be analysed. Fig. 6 represents the aluminium spray measured angle for 8 frames taken at different instants of time. The software used for post-processing the images is Kinovea, an open source software that provides features to analyse images and video.

As clearly shown by the images below, during the experimental test the spray does not maintain the same exit angle. Indeed, during the first part of the injecting phase the aluminium spray angle is very narrow; thus, the spray is concentrated into a restricted area. During the experimental test, the spray becomes wider until it reaches an angle of 44° towards the end of the injection phase. The increase in the spray angle during the experimental test could be conditioned by the liquid aluminium that solidifies at the outlet of the nozzle due to the abrupt decrease in temperature and the solidified aluminium could have modified the shape of the injection.

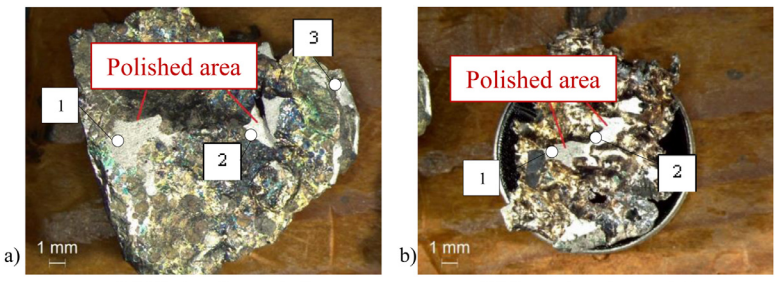

(a) First agglomerated, **(b)** Second agglomerated

Fig. 7. (a) First agglomerated, (b) second agglomerated.

In a system based on the liquid aluminium reaction with water the monitoring of the spray angle is essential because this parameter influences the interaction between the molten aluminium jet and the steam stream; thus, the spray angle conditions the efficiency of the reaction. The efficiency of the system grows with the increase of the spray angle.

3.4. Composition

During the experimental test the aluminium spray falls into a basin of water where it cools down and forms many small flakes. Two different agglomerated of these small flakes are analysed and they are shown in Fig. 7. The results are presented as mass percentage in Tables 4 and 5 for each element, i.e., O, Al, Si.

From Table 4 the analysis of the first agglomerated sample can be observed. analysing the external surface, the table highlights that the percentage of Silica drops to zero while the percentage of Oxygen grows up to 28% of the total weight thanks to the oxidation reaction that takes place when the aluminium spray exits from the nozzle.

Table 4
First agglomerated composition percentage.

Spectrum	O [%]	Al [%]	Si [%]
#1	3.33	95.99	0.68
#2	3.01	94.32	2.67
#3	4.25	92.83	2.92
External surface	28.14	71.86	

Table. 5
Second agglomerated composition percentage.

Spectrum	O [%]	Al [%]	Si [%]
#1	2.13	94.64	3.23
#2	2.4	94.62	2.98

In the other points analysed, i.e., 1,2,3 for the first sample and 1,2 for the second sample, it can be noticed that aluminium has a rate of approximately the 95%; the amount of Oxygen varies in the

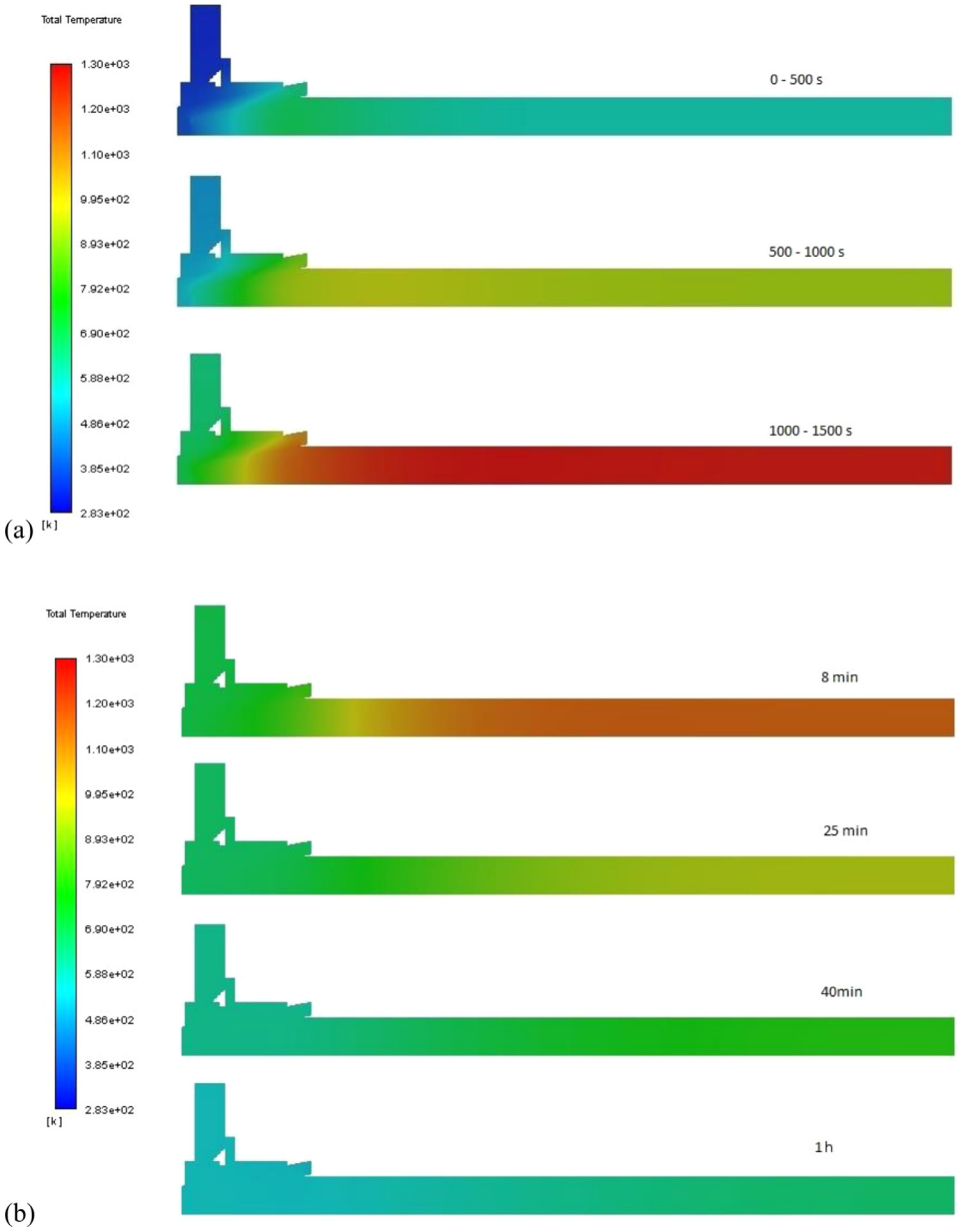

Fig. 8. Contour maps of temperature in the system during the heating (a) and cooling phase (b) at selected times.

range between 2.13% and 4.25%, while the Silica is in the range of 0.68%–3.23%.

3.5. Thermal transients

Figs. 8 and 9 report synthetically the results of the transient thermal analysis. In Fig. 8 temperature maps are reported for both the heating (Fig. 8a) and cooling (Fig. 8b) phases. It can be observed that in the heating phase, predictably, high temperature gradients develop rapidly in the nozzle region, where the presence of multiple materials determines a differentiated response to the thermal input. These gradients are expected to be the main source of thermal stress on the structure. The cooling phase is instead much slower, and the release of heat through the outer surface of the crucible helps to ease the high degree thermal stress on the nozzle region. It is to be noted that the length of the cooling phase is directly linked to the heat transfer coefficients imposed for the cooling phase, which have yet to be compared with an experimental benchmark. Fig. 9 reports the numerical time evolution of temperature during both heating and cooling. The numerical curve has been compared with the experimental values measured by the thermocouple TA2 and the thermal camera, i.e., T_nozzle. It can be seen that the values at the end of the heating phase (t = 1500 s) are in good agreement with the experimental values; thus, the thermal boundary conditions and the source terms adopted for the simulation are suitable for the investigation of this phenomenon. Interestingly, it can be noted that, during the cooling phase, the different boundary condition on the outer surface of the crucible determines a redistribution of the thermal gradients, and the nozzle reaches its maximum temperature 8 min after the start of the cooling process.

3.6. Thermomechanical analysis

Fig. 10 shows the contour map of the Von Mises equivalent stress on the system, in case of steady state condition. The results highlight negligible stresses both in the graphite nose of the melting pot, and in the nozzle. With regard to the threaded nut, the stresses assume a relevant value, about 600 MPa, close to the thread, due to the effect of the constraint from the outer frame, which prevents the radial deformation of the threaded nut.

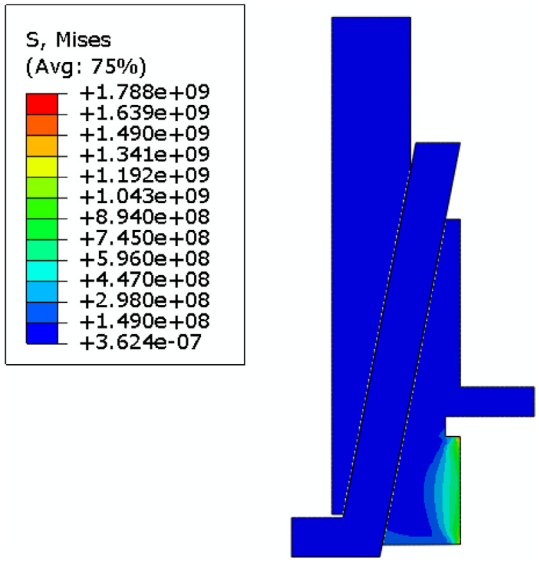

Fig. 10. Contour map of the Von Mises stress in the system.

The negligible stress values on the nose of the melting pot and the on the nozzle comes from the favourable values of the thermal expansion coefficient of their materials (Table 3). The graphite of the melting pot has the lowest coefficient, followed by the carbide ceramic of the nozzle, whose thermal expansion coefficient is lower than that of the titanium of the threaded nut. Thus, each component has enough room for thermal deformation, without any induced critical thermal stresses.

This investigation focused on the steady state condition of the system, since the heating and cooling phases have a low temperature rate that prevents critical peak stresses in the system. However, the investigation

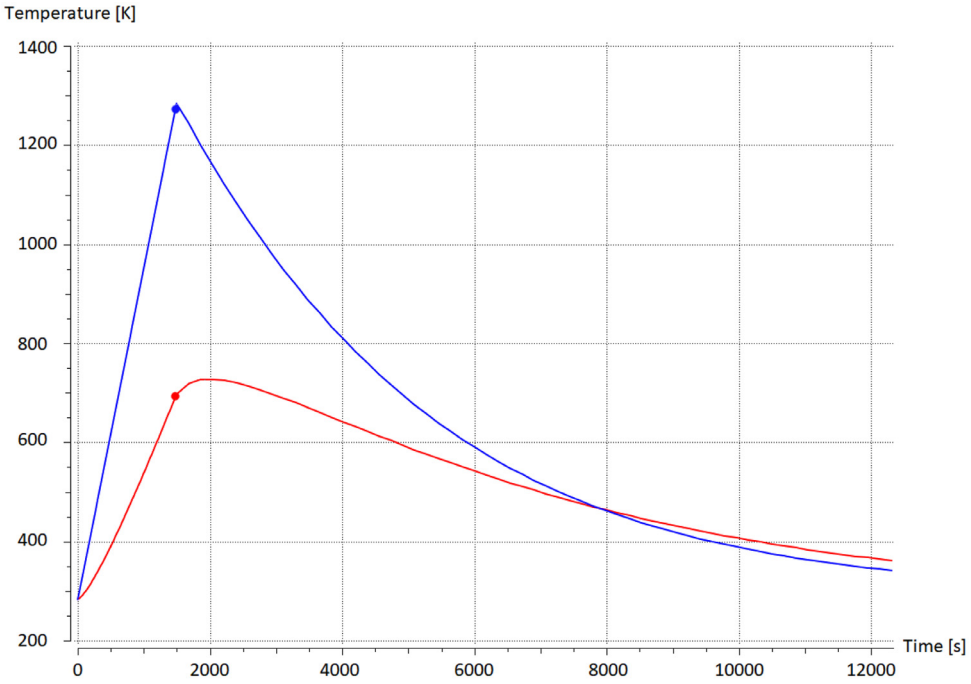

Fig. 9. Time evolution of temperature during heating and cooling, as sampled in the approximate locations of the thermocouples T-A2 (blue line) and T-nozzle (red line). Dots represent experimental values at the end of the heating phase (t = 1500 s). (For interpretation of the references to colour in this figure legend, the reader is referred to the web version of this article.)

will be improved in two directions: first, by including in the model also the external frame, in order to correctly describe all the constraint conditions on the system; second, by considering also the heating and cooling phase corresponding to the start and stop of the system.

4. Conclusion

A combined approach for the analysis of the pressurised injection system for liquid aluminium for a cogeneration system based on the Al−H_2O reaction has been presented. The experimental measurements carried out on an ad − hoc test rig have been used to implement the numerical thermal and structural analyses of the injection nozzle, which is the critical component of the system.

The experimental measurements were employed to determine the temperature in the injection crucible upstream of the nozzle. High speed camera images were used to measure the spray characteristics of the liquid aluminium in terms of spray angle and nozzle external temperature.

The simulation of the temperature distribution of the nozzle analysed the cooling phase of the process which is the most critical part for the component resistance. The numerical results demonstrated to be in good agreement with the measurements and highlighted that the different boundary condition on the outer surface of the crucible determined a redistribution of the thermal gradients, and the nozzle reached its maximum temperature 8 min after the start of the cooling process.

Finally, the temperature distribution calculated with the thermal analysis of the nozzle was used for the structural analysis. The Von Mises equivalent stress was calculated for the most critical temperature condition of the system. The negligible stress values were determined, due to the favourable values of the thermal expansion coefficient of the adopted materials. Simulation proved that each component had enough room for thermal deformation, without any induced critical thermal stresses.

Declaration of Competing Interest

The authors declare that they have no known competing financial interests or personal relationships that could have appeared to influence the work reported in this paper.

References

[1] J. Malinauskaite, H. Jouhara, L. Ahmad, M. Milani, L. Montorsi, M. Venturelli, Energy efficiency in industry: EU and national policies in Italy and the UK, Energy (2019), doi: 10.1016/j.energy.2019.01.130.

[2] N. Lior, Sustainable energy development: the present (2009) situation and possible paths to the future, Energy (2010), doi: 10.1016/j.energy.2010.03.034.

[3] H. Jouhara, N. Khordehgah, S. Almahmoud, B. Delpech, A. Chauhan, S.A. Tassou, Waste heat recovery technologies and applications, Therm. Sci. Eng. Prog. (2018), doi: 10.1016/j.tsep.2018.04.017.

[4] Bakartxo E., Jouhara H., Zuazua J., Al-Mansour F., Plesnik K., Montorsi L., Manzini L., ETEKINA: analysis of the potential for waste heat recovery in three sectors: aluminium low pressure die casting, steel sector and ceramic tiles manufacturing sector, Int. J. Thermofluids, 10.1016/j.ijft.2019.100002.

[5] P.P. Edwards, V.L. Kuznetsov, W.I.F. David, N.P. Brandon, Hydrogen and fuel cells: towards a sustainable energy future, Energy Policy 36 (12) (2008) 4356–4362.

[6] I. Dincer, T.A.H. Ratlamwala, Development of novel renewable energy based hydrogen production systems: a comparative study, Energy Convers. Manag. 72 (2013) 77–87, doi: 10.1016/j.enconman.2012.08.029.

[7] S. Sharma, S.K. Ghoshal, Hydrogen the future transportation fuel: from production to application, Renew. Sustain. Energy Rev. (2014), doi: 10.1016/j.rser.2014.11.093.

[8] İ. Yılmaz, M. İlbaş, M. Taştan, C. Tarhan, Investigation of hydrogen usage in aviation industry, Energy Convers. Manag. 63 (2012) 63–69, doi: 10.1016/j.enconman.2011.12.032.

[9] F. Sorgulu, I. Dincer, A renewable source based hydrogen energy systemfor residential applications, Int. J. Hydrogen Energy 43 (2018) 5842–5851, doi: 10.1016/j.ijhydene.2017.10.101.

[10] J.D. Holladay, J. Hu, D.L. King, Y. Wang, An overview of hydrogen production technologies, Catal. Today 139 (2009) 244–260, doi: 10.1016/j.cattod.2008.08.039.

[11] R. Kothari, D. Buddhi, R.L. Sawhney, Comparison of environmental and economic aspects of various hydrogen production methods, Renew. Sustain. Energy Rev. 12 (2) (2008) 553–563, doi: 10.1016/j.rser.2006.07.012.

[12] J.O. Abe, A.P.I. Popoola, E. Ajenifuja, O.M. Popoola, Hydrogen energy, economy and storage: review and recommendation, Int. J. Hydrogen Energy 44 (2019) 75072-15086, doi: 10.1016/j.ijhydene.2019.04.068.

[13] E.I. Shkolnikov, A.Z. Zhuk, M.S. Vlaskin, Aluminum as energy carrier: feasibility analysis and current technologies overview, Renew. Sustain. Energy Rev. 15 (9) (2011) 4611–4623, doi: 10.1016/j.rser.2011.07.091.

[14] Y. Yavor, S. Goroshin, J.M. Bergthorson, D.L. Frost, R. Stowe, S. Ringuette, Enhanced hydrogen generation from aluminum-water reactions, Int J Hydrogen Energy 38 (35) (2013) 14992–15002.

[15] J.P. Foote, B.R. Thompson, J.T. Lineberry, Combustion of aluminum and steam for underwater propulsion, in: G.D. Roy (Ed.), Advances in Chemical Propulsion: Science to Technology, Office of Naval Research, Arlington, Virginia, USA, 2002, pp. 133–147.

[16] G. Risha, T. Connell, R. Yetter, V. Yang, T. Wood, M. Pfeil, T. Pourpoint, S. Son, Aluminum-ICE (ALICE) propellants for hydrogen generation and propulsion, in: Proceedings of the 45th AIAA/ASME/SAE/ASEE Joint Propulsion Conference & Exhibit, American Institute of Aeronautics and Astronautics, 2009.

[17] J.M. Bergthorson, Y. Yavor, J. Paleck, W. Georges, M. Soo, J. Vickery, S. Goroshin, D.L. Frost, A.J. Higgins, Metal-water combustion for clean propulsion and power generation, Appl. Energy 186 (2017) 13–27, doi: 10.1016/j.apenergy.2016.10.033.

[18] P. Dupiano, D. Stamatis, E.L. Dreizin, Hydrogen production by reacting water with mechanically milled composite aluminum-metal oxide powders, Int. J. Hydrogen Energy 36 (8) (2011) 4781–4791, doi: 10.1016/j.ijhydene.2011.01.062.

[19] W.Z. Gai, W.H. Liu, Z.Y. Deng, J.G. Zhou, Reaction of Al powder with water for hydrogen generation under ambient condition, Int. J. Hydrogen Energy 37 (17) (2012) 13132–13140, doi: 10.1016/j.ijhydene.2012.04.025.

[20] M.W. Beckstead, Correlating aluminum burning times, Combust. Explos. Shock Waves 41 (5) (2005) 533–546.

[21] E.L. Dreizin, Metal-based reactive nanomaterials, Prog. Energy Combust. Sci. 35 (2) (2009) 141-167, doi: 10.1016/j.pecs.2008.09.001.

[22] V. Shmelev, H. Yang, C. Yim, Hydrogen generation by reaction of molten aluminium with water steam, Int. J. Hydrogen Energy 41 (2016) 14562–14572, doi: 10.1016/j.ijhydene.2016.05.277.

[23] F. Franzoni, S. Mercati, M. Milani, L. Montorsi, Operating maps of a combined hydrogen production and power generation system based on aluminum combustion with water, Int. J. Hydrogen Energy 36 (4) (2011) 2803–2816, doi: 10.1016/j.ijhydene.2010.11.064.

[24] S. Mercati, M. Milani, L. Montorsi, F. Paltrinieri, Design of the steam generator in an energy conversion system based on the aluminum combustion with water, Appl. Energy 97 (0) (2012) 686–694, doi: 10.1016/j.apenergy.2012.01.028.

[25] S. Mercati, M. Milani, L. Montorsi, F. Paltrinieri, Optimization of the working cycle for a hydrogen production and power generation plant based on aluminum combustion with water, Int. J. Hydrogen Energy 38 (18) (2013) 7209–7217, doi: 10.1016/j.ijhydene.2013.04.043.

[26] D. Castagnetti, E. Dragoni, G. Scirè Mammano, Elastostatic contact model of rubber-coated truck wheels loaded to the ground, Proc. Inst. Mech. Eng. Part L J. Mater. Des. Appl. 222 (2008) 245–257, doi: 10.1016/j.ijadhadh.2008.01.005.

[27] A. Caffagni, D. Angeli, G.S. Barozzi, S. Polidoro, A revised approach for one-dimensional time-dependent heat conduction in a slab, J. Heat Transf. 135 (2013) Art. no. 31301, doi: 10.1115/1.4007982.

[28] ANSYS® Fluent Academic Research, Release 18.1

[29] Fundamentals of Heat and Mass Transfer, Bergman T.L., DeWitt D.P., Incropera F.P., John Wiley & Sons Inc, 6th ed.

[30] Dassault Systems and Simulia. Abaqus 16.0